Journal of Intelligent Material Systems and Structures

Original Article

Journal of Intelligent Material Systems and Structures
1–17

DOI: 10.1177/1045389X18758191
journals.sagepub.com/home/jim
SAGE

Buckling analysis of skew magneto-electro-elastic plates under in-plane loading

MC Kiran and Subhaschandra Kattimani

Abstract

This article deals with the study of buckling behaviour of multilayered skew magneto-electro-elastic plate under uniaxial and biaxial in-plane loadings. The skew edges of the skew magneto-electro-elastic plate are obtained by transforming the local skew coordinate to the global using a transformation matrix. The displacement fields corresponding to the first-order shear deformation theory along with constitutive equations of magneto-electro-elastic materials are used to develop a finite element model. The finite element model encompasses the coupling between electric, magnetic and elastic fields. The in-plane stress distribution within the skew magneto-electro-elastic plate due to the enacted force is considered to be equivalent to the applied in-plane compressive loads in the pre-buckling range. This stress distribution is used to derive the potential energy functional of the skew magneto-electro-elastic plate. The non-dimensional critical buckling load is attained from the solution of the allied linear eigenvalue problem. Influence of skew angle, stacking sequence, span-to-thickness ratio, aspect ratio and boundary condition on the critical buckling load and their corresponding mode shapes is investigated.

Keywords

Skew plate, magneto-electro-elastic plate, buckling, stability behaviour, critical buckling load, in-plane loads

Introduction

Recently, the demand for multifunctional structures in many engineering applications has been increasing rapidly. One such material possessing multifunctional capabilities is magneto-electro-elastic (MEE) composite. The MEE composites find their presence in smart structural components, electronic probes, high-frequency devices, sensors, actuators and so on and hold its scope in many future applications. These composites are formed from the combination of two distinct phases such as piezoelectric and magnetostrictive material. A new product property (Van Suchtelen, 1972) arising from the combination of two such distinct phases is called magneto-electric coupling and is observed only in MEE composites. However, the individual phases, that is, piezoelectric and magnetostrictive of the composite, exhibit electro-elastic and magneto-elastic coupling, respectively. The first production of MEE composite using unidirectional solidification (Boomgaard and Born, 1978) was followed by numerous analytical, finite element (FE) and many more mathematical models to understand the characteristic behaviour of MEE structures. Studies related to free vibration, static, buckling, nonlinear, dynamic behaviour and so on have gained more importance with the increase in the application spectrum of MEE composites.

The free vibration characteristics and static behaviour under various loading conditions of MEE plate are extensively reported in the literature (Bhangale and Ganesan, 2005; Buchanan, 2004; Chen et al., 2014; Guan, 2012; Kondaiah et al., 2015; Kondaiah and Shankar, 2017; Lage et al., 2004; Moita et al., 2009; Ramirez et al., 2006; Wang et al., 2003). Pan and his co-researchers (Pan, 2001; Pan and Han, 2005; Pan and Heyliger, 2002, 2003) laid down the benchmark solutions for free vibration and static studies of MEE plate. Milazzo (2014a, 2014b) provided key contributions in understanding the large deflection and free vibration aspects of MEE plate. Active constrained layered damping treatment was imparted for the effective control of nonlinear vibrations in MEE plates and shells by Kattimani and Ray (2014a, 2014b, 2015). Liu et al.

National Institute of Technology Karnataka, Surathkal, India

Corresponding author:
Subhaschandra Kattimani, National Institute of Technology Karnataka, Srinivasnagar PO, Surathkal 575025, India.
Email: sck@nitk.ac.in

(2016) obtained higher order solutions for MEE plate with non-uniform materials using scaled boundary FE method. Vinyas and Kattimani (2017a, 2017b, 2017c) analysed the static behaviour of stepped functionally graded MEE plates and beams subjected to various thermal loading. The geometrically nonlinear vibrations of multiferroic composite plate and shell were analysed by Kattimani (2017). Recently, the refined models involving the Carrera unified formulation has facilitated the evaluation of various approaches such as the layerwise models and equivalent single-layer models in the unified formulation (Carrera et al., 2009, 2018; Milazzo, 2016; Ottavio and Carrera, 2010).

The stability characteristics of MEE plate have recently sought much attention from researchers. Kumaravel et al. (2007, 2010) were the first to report buckling behaviour under thermal environment for layered and functionally graded MEE beams and cylinders. The stability characteristic of MEE plate resting on Pasternak elastic foundation was investigated by Li (2014). Considering the surface effects, Xu et al. (2016) analysed the bending and buckling behaviour of MEE beams. Ebrahimi et al. (2016a, 2016b, 2016c) used nonlocal theory to investigate the stability behaviour of MEE beams, nano beams and nano plates. Meanwhile, Li et al. (2016) studied the buckling behaviour of functionally graded nano beam using nonlocal theory. Free vibration and biaxial buckling of MEE micro plates were analysed using modified strain gradient theory by Jamalpoor et al. (2017).

A plate with skewness introduced as a geometrical modification exhibited enhanced structural strength characteristics (Durvasula, 1971; Mizusawa et al., 1998; Wang et al., 1992). Many studies involving the buckling of skew plates were reported by several researchers. Wang (1997) investigated the buckling of fibre-reinforced composite skew plates using first-order shear deformation theory (FSDT) in conjunction with B-spline Rayleigh–Ritz method. A new method based on higher order shear deformation theory was proposed by Chakrabarti and Sheikh (2010) to analyse the buckling behaviour of laminated composite plates. The corner stresses influencing the buckling behaviour of skew composite plates subjected to in-plane loading were analysed by Daripa and Singha (2009). Nonlinear stability behaviour of composite skew plates was evaluated by Kumar et al. (2016). Upadhyay and Shukla (2013, 2014) investigated the post-buckling behaviour of laminated composite skew pales under combined in-plane loadings. Jaberzadeh and Azhari (2014) presented the local stability characteristics of viscoelastic composite skew plates.

The comprehensive literature review suggests that the extensive research pertaining to free vibration, static studies, nonlinear behaviour, dynamic characteristics of layered and functionally graded MEE plates, beams and shells have been extensively published. In addition, studies concerned with buckling behaviour of MEE plates resting on an elastic foundation are recently reported. Furthermore, the buckling behaviour of the laminated skew composite plate is also well reported. However, to the best of authors' knowledge, studies related to buckling of multilayered skew MEE (SMEE) plate are unavailable in the open literature. Consequently, this article presents an FE model based on FSDT to assess the stability characteristics of the multilayered SMEE plate. The stability characteristics are well presented in terms of non-dimensional critical buckling load and their corresponding mode shapes which are obtained by solving a linear eigenvalue problem. In addition, parametric studies such as the effect of skew angle, uniaxial and biaxial compression, aspect ratio, span-to-thickness ratio and boundary conditions on buckling behaviour of SMEE plate are studied in detail.

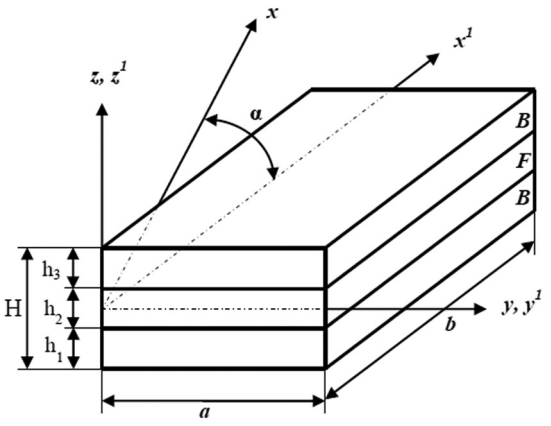

Figure 1. Illustration of three-layered SMEE plate.

Problem description and governing equation

A schematic diagram of a three-layered SMEE plate is illustrated in Figure 1. The length, the width and the total thickness of the plate are a, b and H, respectively. α is the skew angle of the SMEE plate. The SMEE plate consists of three layers of equal thickness h_i (i = 1, 2, 3). The top and the bottom layers are made of identical material, either piezoelectric ($BaTiO_3$) commonly represented by B or magnetostrictive ($CoFe_2O_4$) commonly represented by F while the middle layer is of the other material, that is, magnetostrictive or piezoelectric. Based on the stacking sequence of the material, the SMEE composite is called B/F/B or F/B/F indicating the top/middle/bottom layer, respectively, wherein B refers to barium titanate while F refers to cobalt ferrite. The SMEE plate is subjected to uniaxial and biaxial in-plane loads as shown in Figure 2.

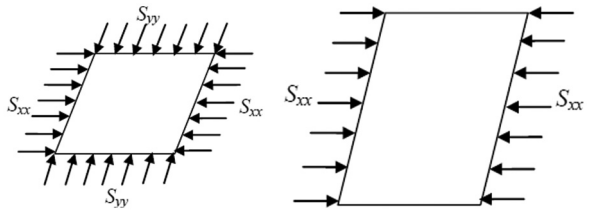

Figure 2. SMEE plate subjected to biaxial and uniaxial compression modes.

The displacement field of such SMEE plate is considered as a first-order expansion of Taylor's series of the midplane variables with respect to the plate thickness. Hence, the displacement fields are given by

$$u = u_0 + z\theta_x, v = v_0 + z\theta_y, w = w_0 \tag{1}$$

where u_0, v_0 and w_0 are the initial displacements at the midplane, and θ_x and θ_y are the rotations of the line initially normal to the midplane relative to the y- and x-axis, respectively. For the ease of computation, the displacement components are split into translational and rotational displacement vectors as follows

$$\{d_t\} = [\,u_0 \quad v_0 \quad w_0\,]^T, \{d_r\} = [\,\theta_x \quad \theta_y\,]^T \tag{2}$$

Since thin plate analysis is involved, to avoid shear locking, selective integration scheme is used. In addition, to emphasize the effect of transverse shear deformation, the strain at any point in the SMEE plate is divided into bending strain vector and shear strain vector represented as follows

$$\begin{aligned} \{\varepsilon\} &= \{\,\varepsilon_x \quad \varepsilon_y \quad \varepsilon_z \quad \gamma_{xy} \quad \gamma_{xz} \quad \gamma_{yz}\,\}^T \\ \{\varepsilon_b\} &= \{\,\varepsilon_x \quad \varepsilon_y \quad \varepsilon_z \quad \gamma_{xy}\,\}^T, \{\varepsilon_s\} = [\,\gamma_{xz} \quad \gamma_{yz}\,]^T \end{aligned} \tag{3}$$

Using the displacement field from equation (1) and the strain components in equation (3) along with the strain–displacement relations, the state of in-plane, transverse normal and transverse shear stress components at any point in the plate can be expressed as

$$\{\varepsilon_b\} = \{\varepsilon_{bt}\} + [Z_1]\{\varepsilon_{br}\}, \{\varepsilon_s\} = \{\varepsilon_{st}\} + [Z_2]\{\varepsilon_{sr}\} \tag{4}$$

in which $[Z_1]$ and $[Z_2]$ are the transformation matrices given as

$$[Z_1] = \begin{bmatrix} z & 0 & 0 & 0 \\ 0 & z & 0 & 0 \\ 0 & 0 & 0 & 0 \\ 0 & 0 & 0 & z \end{bmatrix}, [Z_2] = \begin{bmatrix} 1 & 0 \\ 0 & 1 \end{bmatrix} \tag{5}$$

Correspondingly, the various strain components appearing in equation (4) are given by

$$\begin{aligned} \{\varepsilon_{bt}\} &= \left[\frac{\partial u_0}{\partial x} \;\; \frac{\partial v_0}{\partial y} \;\; 0 \;\; \frac{\partial u_0}{\partial y} + \frac{\partial v_0}{\partial x}\right]^T, \{\varepsilon_{st}\} = \left[\frac{\partial w_0}{\partial x} \;\; \frac{\partial w_0}{\partial y}\right]^T \\ \{\varepsilon_{br}\} &= \left[\frac{\partial \theta_x}{\partial x} \;\; \frac{\partial \theta_y}{\partial y} \;\; 0 \;\; \frac{\partial \theta_x}{\partial y} + \frac{\partial \theta_y}{\partial x}\right]^T, \{\varepsilon_{sr}\} = [\,\theta_x \quad \theta_y\,]^T \end{aligned} \tag{6}$$

Analogous to the strain vectors presented in equation (3), the stress state at any given point in the SMEE plate can be expressed as follows

$$\{\sigma_b\} = [\,\sigma_x \quad \sigma_y \quad \sigma_z \quad \tau_{xy}\,]^T, \{\sigma_s\} = [\,\tau_{xz} \quad \tau_{yz}\,]^T \tag{7}$$

wherein σ_x, σ_y and σ_z along the x-, y- and z-directions are the corresponding normal stresses; the in-plane shear stress component is τ_{xy}; τ_{xz} and τ_{yz} are the out-of-plane shear stress components along the xz- and yz-directions, respectively. Considering the effect of coupled fields, the constitutive equations for the SMEE plate are given by

$$\{\sigma_b^k\} = [\bar{C}_b^k]\{\varepsilon_b^k\} - \{e_b^k\}E_z - \{q_b^k\}H_z, \{\sigma_s^k\} = [\bar{C}_s^k]\{\varepsilon_s^k\} \tag{8a}$$

$$D_z = \{e_b^k\}^T\{\varepsilon_b^k\} + \xi_{33}^k E_z + d_{33}H_z \tag{8b}$$

$$B_z = \{q_b^k\}^T\{\varepsilon_b^k\} + d_{33}^k E_z + \mu_{33}H_z \tag{8c}$$

Here, $k = 1, 2, 3$ denotes the layer number initiating from the bottom layer of the SMEE plate and

$$[\bar{C}_b^k] = \begin{bmatrix} \bar{C}_{11}^k & \bar{C}_{12}^k & \bar{C}_{13}^k & 0 \\ \bar{C}_{12}^k & \bar{C}_{22}^k & \bar{C}_{23}^k & 0 \\ \bar{C}_{13}^k & \bar{C}_{23}^k & \bar{C}_{33}^k & 0 \\ 0 & 0 & 0 & \bar{C}_{66}^k \end{bmatrix}, [\bar{C}_s^k] = \begin{bmatrix} \bar{C}_{55}^k & \bar{C}_{45}^k \\ \bar{C}_{45}^k & \bar{C}_{44}^k \end{bmatrix} \tag{9}$$

where $[\bar{C}_b^k]$ and $[\bar{C}_s^k]$ represent the transformed coefficient matrices, ξ_{33}^k is the dielectric constant, μ_{33} represents the magnetic permeability coefficient and d_{33} is the electromagnetic coefficient. Since the plate is considered to be thin, the electric displacement, the electric field, the magnetic induction and the magnetic field along the z-direction are only considered and represented by D_z, E_z, B_z and H_z, respectively. The electric coefficient matrix $\{e_b^k\}$ and the magnetic coefficient matrix $\{q_b^k\}$ are given by

$$\begin{aligned} \{e_b^k\} &= \{\,e_{31} \quad e_{32} \quad e_{33} \quad e_{36}\,\}^T, \\ \{q_b^k\} &= \{\,q_{31} \quad q_{32} \quad q_{33} \quad q_{36}\,\}^T \end{aligned} \tag{10}$$

Using the principle of virtual work, the governing equations for the SMEE plate can be established as

$$\delta\Pi = \delta U + \delta V = 0 \tag{11}$$

wherein

$$\delta U = \sum_{k=1}^{3} \left(\int_{\Lambda^k} \delta\{\varepsilon_b^k\}\{\sigma_b^k\} \mathrm{d}\Lambda^k + \int_{\Lambda^k} \delta\{\varepsilon_s^k\}\{\sigma_s^k\} \mathrm{d}\Lambda^k + \int_{\Lambda^k} \delta\{d_t\}^T \rho^k \{\ddot{d}_t\} \mathrm{d}\Lambda^k \right) - \int_{\Lambda^t} \delta E_z^t D_z^t \mathrm{d}\Lambda^t - \int_{\Lambda^b} \delta E_z^b D_z^b \mathrm{d}\Lambda^b - \int_{\Lambda^m} \delta H_z B_z \mathrm{d}\Lambda^m - \int_{A^{el}} \delta\{d_t\}^T F_t \mathrm{d}A^{el} \quad (12)$$

Meanwhile, the work accounted for applied in-plane loads can be expressed as

$$\delta V = \int_0^a \int_0^b \begin{bmatrix} \frac{\partial w}{\partial x} \\ \frac{\partial w}{\partial y} \end{bmatrix}^T [\sigma_0] \begin{bmatrix} \frac{\partial w}{\partial x} \\ \frac{\partial w}{\partial y} \end{bmatrix} \mathrm{d}x\mathrm{d}y \quad (13)$$

where Λ^k ($k = 1, 2, 3$) designates the volume of the respective layer, F_t corresponds to the applied surface traction force on the top surface area A^{el} and ρ^k denotes the mass density of the kth layer. Λ^t and Λ^b represent the volume of the top and bottom piezoelectric, respectively, while the middle magnetostrictive layer is represented by Λ^m. $[\sigma_0]$ is the initial stress matrix. E_z^t, E_z^b and D_z^t, D_z^b are the electric fields and the electric displacements of the top and the bottom layers of the SMEE plate, respectively, whereas H_z^m and B_z^m are the magnetic field and magnetic induction in the middle layer, respectively. The transverse electric field (E_z) is related to the electric potential and the transverse magnetic field (H_z) is related to the magnetic potential in accordance with Maxwell's equation as follows

$$E_z^t = -\frac{\partial \phi^t}{\partial z}, E_z^b = -\frac{\partial \phi^b}{\partial z} \text{ and } H_z^m = -\frac{\partial \psi^m}{\partial z} \quad (14)$$

where *t, b* and *m* represent the top, bottom and middle layers of the SMEE plate, respectively, depending on the stacking sequence of the layers. The interface linking piezoelectric and magnetostrictive layers is assumed to be properly grounded. Since the SMEE plate layers possess a very small thickness, the variation in the electric and magnetic potential across the thickness can be suitably assumed to be linear. Correspondingly, the electric potential functions ϕ^t and ϕ^b pertaining to the top and the bottom piezoelectric layers and ψ^m the magnetic potential pertaining to the middle magnetostrictive layer of the SMEE plate (Kattimani, 2015) can be represented as

$$\phi^t = \frac{z - z_b}{h}\phi_1, \phi^b = -\frac{z - h_2}{h}\phi_2, \text{ and } \psi^m = \frac{z - h_2}{h}\bar{\psi} \quad (15)$$

where z_b denotes the z-coordinate of the bottom surface of the top piezoelectric layer (Kattimani, 2015); h_2 represents the z-coordinate of the top face of the bottom piezoelectric layer; the electric potentials ϕ_1 and ϕ_2 correspond to the top and the bottom surfaces of the top and the bottom piezoelectric layers, respectively (Kattimani and Ray, 2014a). The magnetic potential on the bottom face of the middle magnetostrictive layer is indicated by $\bar{\psi}$.

FE formulation

The SMEE plate is discretized using four-noded quadrilateral elements. Considering equation (2), the displacement vectors in generalized form $\{d_{ti}\}$ and $\{d_{ri}\}$ are linked with the ith node (where $i = 1, 2, 3, 4$) of an element and can be articulated as

$$\{d_{ti}\} = [\, u_{0i} \quad v_{0i} \quad w_{0i} \,]^T \text{ and } \{d_{ri}\} = [\, \theta_{xi} \quad \theta_{yi} \,]^T \quad (16)$$

At any given point within the element, the displacement vectors in generalized form $\{d_t\}$ and $\{d_r\}$, the generalized electric potential vector $\{\phi\}$ and the generalized magnetic potential vector $\{\psi\}$ can be expressed in terms of nodal generalized displacement vectors $\{d_t^{el}\}$ and $\{d_r^{el}\}$, the nodal magnetic potential vector $\{\psi^{el}\}$ and the nodal electric potential vector $\{\phi^{el}\}$, respectively (Kattimani, 2015), as follows

$$\begin{aligned} &\{d_t\} = [n_t]\{d_t^{el}\}, \{d_r\} = [n_r]\{d_r^{el}\}, \\ &\{\phi\} = [\, \phi_1 \; \phi_2 \,]^T = [n_\phi]\{\phi^{el}\} \\ &\{\psi\} = [\, \psi_1 \; \psi_2 \,]^T = [n_\psi]\{\psi^{el}\} \text{ and } \{\psi^m\} = [n_\psi^m]\{\psi_m^{el}\} \end{aligned} \quad (17)$$

in which

$$\begin{aligned} &\{d_t^{el}\} = \left[\{d_{t1}^{el}\}^T \quad \{d_{t2}^{el}\}^T \quad \ldots \quad \{d_{t4}^{el}\}^T \right]^T, \\ &\{d_r^{el}\} = \left[\{d_{r1}^{el}\}^T \quad \{d_{r2}^{el}\}^T \quad \ldots \quad \{d_{r4}^{el}\}^T \right]^T \\ &\{\phi^{el}\} = \{\, \phi_{11} \quad \phi_{21} \quad \phi_{12} \quad \phi_{22} \quad \ldots \quad \phi_{14} \quad \phi_{24} \,\}^T, \\ &\{\bar{\psi}^{el}\} = \{\, \bar{\psi}_1 \quad \bar{\psi}_2 \quad \ldots \quad \bar{\psi}_4 \,\}^T \\ &[n_t] = [\, n_{t1} \quad n_{t2} \quad \ldots \quad n_{t4} \,]^T, [n_r] = [\, n_{r1} \quad n_{r2} \quad \ldots \quad n_{r4} \,]^T \\ &[n_\phi] = \begin{bmatrix} n_{\phi_{11}} & 0 & n_{\phi_{12}} & 0 & & n_{\phi_{14}} & 0 \\ 0 & n_{\phi_{21}} & 0 & n_{\phi_{22}} & \ldots & 0 & n_{\phi_{24}} \end{bmatrix}^T, \\ &[n_\psi] = [\, n_{\psi 1} \quad n_{\psi 2} \quad \ldots \quad n_{\psi 4} \,]^T \\ &n_{ti} = N_i I_t, \; n_{ri} = N_i I_r \end{aligned} \quad (18)$$

where $[n_t]$, $[n_r]$, $[n_\phi]$ and $[n_\psi]$ are the shape function matrices while I_t and I_r are the identity matrices, respectively (Kattimani, 2015). The shape function N_i corresponding to the natural coordinate is linked with the ith node. The degrees of freedom corresponding to electric potential and magnetic potential are ϕ_{1i}, ϕ_{2i} (where $i = 1, 2, 3, 4$) and $\bar{\psi}_i$, respectively. Using equations (12) to (16), the transverse electric field for the top and the bottom layers (E_z^t, E_z^b) and the transverse magnetic field for the middle layer (H_z^m) are given by

$$E_z^t = -\frac{1}{h}[1 \quad 0][n_\phi]\{\phi^{el}\},$$
$$E_z^b = -\frac{1}{h}[0 \quad 1][n_\phi]\{\phi^{el}\}, \text{ and } H_z^m = -\frac{1}{h}[n_\psi]\{\psi^{el}\} \tag{19}$$

Now, considering equations (4) and (16), the strain vectors in generalized form at any given point in the element can be presented in the form of nodal generalized strain vectors as

$$\begin{aligned}\{\varepsilon_{bt}\} &= [b_{bt}]\{d_t^{el}\}, \{\varepsilon_{br}\} = [b_{br}]\{d_r^{el}\} \\ \{\varepsilon_{st}\} &= [b_{st}]\{d_t^{el}\}, \{\varepsilon_{sr}\} = [b_{sr}]\{d_r^{el}\}\end{aligned} \tag{20}$$

in which $[b_{tb}]$, $[b_{rb}]$, $[b_{ts}]$ and $[b_{rs}]$ are the nodal strain–displacement matrices. Substituting equations (4), (10), (13), (19) and (20) into equation (11) and simplifying, we obtain the elemental equations of motion for the SMEE plate as follows

$$\begin{aligned}[M^{el}]\{\ddot{d}_t^{el}\} + [k_{tt}^{el}]\{d_t^{el}\} + [k_{tr}^{el}]\{d_r^{el}\} + [k_{t\phi}^{el}]\{\phi^{el}\} \\ + [k_{t\psi}^{el}]\{\psi^{el}\} + [k_G^{el}]\{d_t\} = \{F_t^{el}\}\end{aligned} \tag{21}$$

$$[k_{tr}^{el}]^T\{d_t^{el}\} + [k_{rr}^{el}]\{d_r^{el}\} + [k_{r\phi}^{el}]\{\phi^{el}\} + [k_{r\psi}^{el}]\{\psi^{el}\} = 0 \tag{22}$$

$$[k_{t\phi}^{el}]^T\{d_t^{el}\} + [k_{r\phi}^{el}]^T\{d_r^{el}\} - [k_{\phi\phi}^{el}]\{\phi^{el}\} = 0 \tag{23}$$

$$[k_{t\psi}^{el}]^T\{d_t^{el}\} + [k_{r\psi}^{el}]^T\{d_r^{el}\} - [k_{\psi\psi}^{el}]\{\psi^{el}\} = 0 \tag{24}$$

The matrices and the vectors displayed in equations (21) to (24) are the elemental mass matrix $[M^{el}]$ and the elemental elastic stiffness matrices $[k_{tt}^{el}]$, $[k_{tr}^{el}]$ and $[k_{rr}^{el}]$; the elemental electro-elastic coupling stiffness and magneto-elastic coupling stiffness matrices are $[k_{t\phi}^{el}]$, $[k_{r\phi}^{el}]$ and $[k_{t\psi}^{el}]$, $[k_{r\psi}^{el}]$, respectively; $[k_G^{el}]$ is the elemental geometric stiffness matrix; $\{F_t^{el}\}$ is the elemental mechanical load vector; $[k_{\phi\phi}^{el}]$ and $[k_{\psi\psi}^{el}]$ are the elemental electric and elemental magnetic stiffness matrices, respectively. The elemental matrices and vectors are given by

$$[k_{tt}^{el}] = [k_{tb}^{el}] + [k_{ts}^{el}], [k_{tr}^{el}] = [k_{trb}^{el}] + [k_{trs}^{el}], [k_{rr}^{el}] = [k_{rrb}^{el}] + [k_{rrs}^{el}]$$

$$[k_{t\phi}^{el}] = [k_{\phi t}^{el}]^T, [k_{t\psi}^{el}] = [k_{\psi t}^{el}]^T, [k_{t\phi}^{el}] = \int_0^{a_{el}}\int_0^{b_{el}} [b_{tb}]^T[D_{t\phi}][n_\phi]\mathrm{d}x\mathrm{d}y$$

$$[k_{r\phi}^{el}] = \int_0^{a_{el}}\int_0^{b_{el}} [b_{rb}]^T[D_{r\phi}][n_\phi]\mathrm{d}x\mathrm{d}y,$$

$$[k_{t\psi}^{el}] = \int_0^{a_{el}}\int_0^{b_{el}} [b_{tb}]^T[D_{t\psi}][n_\psi]\mathrm{d}x\mathrm{d}y$$

$$[k_{r\psi}^{el}] = \int_0^{a_{el}}\int_0^{b_{el}} [b_{rb}]^T[D_{r\psi}][n_\psi]\mathrm{d}x\mathrm{d}y,$$

$$[k_{\phi\phi}^{el}] = \int_0^{a_{el}}\int_0^{b_{el}} [n_\phi]^T[D_{\phi\phi}][n_\phi]\mathrm{d}x\mathrm{d}y$$

$$[k_{\psi\psi}^{el}] = \int_0^{a_{el}}\int_0^{b_{el}} [n_\psi]^T[D_{\psi\psi}][n_\psi]\mathrm{d}x\mathrm{d}y, \tag{25}$$

$$[k_G^{el}] = \int_0^{a_{el}}\int_0^{b_{el}} [b_G]^T[\sigma_0][b_G]\mathrm{d}x\mathrm{d}y$$

where $[D_{t\phi}]$, $[D_{r\phi}]$, $[D_{t\psi}]$, $[D_{r\psi}]$, $[D_{\phi\phi}]$ and $[D_{\psi\psi}]$ are the rigidity matrices appearing in equation (25) and are given as follows

$$[D_{t\phi}] = \int_{h_3}^{h_4}\{e_b\}\frac{1}{h}[1 \quad 0]\,dz + \int_{h_1}^{h_2}\{e_b\}\frac{1}{h}[1 \quad 0]\,dz,$$

$$[D_{t\psi}] = \int_{h_2}^{h_3}\{q_b\}\frac{1}{h}\,dz$$

$$[D_{r\phi}] = \int_{h_3}^{h_4}[z_1]^T\{e_b\}\frac{1}{h}[1 \quad 0]\mathrm{d}z + \int_{h_1}^{h_2}[z_1]^T\{e_b\}\frac{1}{h}[1 \quad 0]\mathrm{d}z,$$

$$[D_{r\psi}] = \int_{h_2}^{h_3}[z_1]^T\{q_b\}\frac{1}{h}\,\mathrm{d}z, \; [D_{\phi\phi}] = \frac{\varepsilon_{33}}{h}\begin{bmatrix}1 & 0\\ 0 & 1\end{bmatrix},$$

$$D_{\psi\psi} = \frac{1}{h}\mu_{33}, \; [\sigma_0] = \begin{bmatrix}\sigma_{xx}^0 & \sigma_{xy}^0\\ \sigma_{xy}^0 & \sigma_{yy}^0\end{bmatrix}$$

Skew boundary transformation

In case of skew MEE plates, the supported adjacent edges of the boundary element are not parallel to the global axes (x, y, z). Hence, to consider the boundary conditions at the skew edges of the plate, the displacements u^1, v^1 and w^1 at any point on the skew edges of the local coordinates must be restrained along the x^1-, y^1- and z^1-directions. The boundary conditions can be specified conveniently by transforming the element matrices corresponding to the global axis to the local axis along the edges. A transformation relation can be expressed between the local degrees of freedom and the global degrees of freedom for the generalized displacement vectors of a point lying on the skew edges of the plate as follows

$$\{d_t\} = [L_t]\{d_t^1\}, \{d_r\} = [L_r]\{d_r^1\} \tag{26}$$

$$\{d_t^1\} = [u_0^1 \quad v_0^1 \quad w_0^1]^T, \{d_r^1\} = [\theta_x^1 \quad \theta_y^1 \quad \theta_z^1 \quad \phi_z^1]^T \tag{27}$$

where $\{d_t\}$, $\{d_r\}$ and $\{d_t^1\}$, $\{d_r^1\}$ are the displacements on the global and the local edge coordinate system,

respectively. $[L_t]$ and $[L_r]$ are the transformation matrices for a node on the skew boundary and are given by

$$[L_t] = \begin{bmatrix} c & s & 0 \\ -s & c & 0 \\ 0 & 0 & 1 \end{bmatrix}, [L_r] = \begin{bmatrix} c & s \\ -s & c \end{bmatrix} \tag{28}$$

in which $c = \cos\alpha$ and $s = \sin\alpha$, and the skew angle of the plate is α. It may be noted that for the nodes which do not lie on the skew edges, the transformation from global coordinates to the local coordinates is not required. The transformation matrices in such cases are the diagonal matrices in which the values of the principle diagonal elements are unity. Thus, considering equation (25), the elemental stiffness matrices of the element containing the nodes laying on the skew edges are given as follows

$$\begin{aligned} [\bar{k}_{tt}^{el}] &= [T_1]^T[k_{tt}^{el}][T_1], [\bar{k}_{tr}^{el}] = [T_1]^T[k_{tr}^{el}][T_2] \\ [\bar{k}_{rr}^{el}] &= [T_2]^T[k_{rr}^{el}][T_2], [M^{el}] = [T_1]^T[M^{el}][T_1] \\ [\bar{k}_{G}^{el}] &= [T_2]^T[k_{G}^{el}][T_2] \end{aligned} \tag{29}$$

where the transformation matrices $[T_1]$ and $[T_2]$ are given by

$$[T_1] = \begin{bmatrix} [L_t] & \tilde{o} & \tilde{o} & \tilde{o} \\ \tilde{o} & [L_t] & \tilde{o} & \tilde{o} \\ \tilde{o} & \tilde{o} & [L_t] & \tilde{o} \\ \tilde{o} & \tilde{o} & \tilde{o} & [L_t] \end{bmatrix},$$

$$[T_2] = \begin{bmatrix} [L_r] & \breve{o} & \breve{o} & \breve{o} \\ \breve{o} & [L_r] & \breve{o} & \breve{o} \\ \breve{o} & \breve{o} & [L_r] & \breve{o} \\ \breve{o} & \breve{o} & \breve{o} & [L_r] \end{bmatrix} \tag{30}$$

in which $\tilde{o}$ and $\breve{o}$ are the (3×3) and (2×2) null matrices, respectively, and the number of $[L_t]$ and $[L_r]$ matrices is equal to the number of nodes in the element.

The global equations of motion are obtained assembling the elemental equations of motion of the SMEE plate as follows

$$[M]\{\ddot{d}_t\} + [k_{tt}^g]\{d_t\} + [k_{tr}^g]\{d_r\} + [k_{t\phi}^g]\{\phi\} + [k_{t\psi}^g]\{\psi\} + [K_G]\{d_t\} = \{F_t\} \tag{31}$$

$$[k_{tr}^g]^T\{d_t\} + [k_{rr}^g]\{d_r\} + [k_{r\phi}^g]\{\phi\} + [k_{r\psi}^g]\{\psi\} = 0 \tag{32}$$

$$[k_{t\phi}^g]^T\{d_t\} + [k_{r\phi}^g]^T\{d_r\} - [k_{\phi\phi}^g]\{\phi\} = 0 \tag{33}$$

$$[k_{t\psi}^g]^T\{d_t\} + [k_{r\psi}^g]^T\{d_r\} - [k_{\psi\psi}^g]\{\psi\} = 0 \tag{34}$$

where $[M]$ is the global mass matrix; $[k_{tt}^g]$, $[k_{tr}^g]$ and $[k_{rr}^g]$ are the elastic global stiffness matrices; $[k_{t\phi}^g]$ and $[k_{r\phi}^g]$ are the electro-elastic coupling global stiffness matrices; $[k_{t\psi}^g]$ and $[k_{r\psi}^g]$ are the magneto-elastic coupling global stiffness matrices; $[K_G]$ is the global geometric stiffness matrix; $\{F_t\}$ is the global mechanical load vector; $[k_{\phi\phi}^g]$ and $[k_{\psi\psi}^g]$ are the global electric and the global magnetic stiffness matrices, respectively. The global equations of motion (equations (31) to (34)) to obtain the global generalized displacement vectors $\{d_t\}$ and $\{d_r\}$ by condensing the global degrees of freedom for $\{\phi\}$ and $\{\psi\}$ in terms of $\{d_r\}$ can be solved as follows

$$\begin{aligned} \{\psi\} &= [k_{\psi\psi}^g]^{-1}[k_{t\psi}^g]^T\{d_t\} + [k_{\psi\psi}^g]^{-1}[k_{r\psi}^g]^T\{d_r\} \\ \{\phi\} &= [k_{\phi\phi}^g]^{-1}[k_{t\phi}^g]^T\{d_t\} + [k_{\phi\phi}^g]^{-1}[k_{r\phi}^g]^T\{d_r\} \\ \{d_r\} &= -[K_3]^{-1}[K_2]^T\{d_t\} \end{aligned} \tag{35}$$

Now, substituting equation (35) into equation (31) and upon simplification, we obtain the global equations of motion in terms of the global translational degrees of freedom as follows

$$\begin{aligned} [M]\{\ddot{d}_t\} + \left([K_1] - [K_2][K_3]^{-1}[K_2]^T\right)\{d_t\} \\ + [K_G]\{d_t\} = \{F_t\} \\ [M]\{\ddot{d}_t\} + [K]\{d_t\} + [K_G]\{d_t\} = \{F_t\} \\ [K] = \left([K_1] - [K_2][K_3]^{-1}[K_2]^T\right) \end{aligned} \tag{36}$$

where the global aggrandized matrices are given as follows

$$\begin{aligned} [K_1] &= [k_{tt}^g] + [k_{t\phi}^g][k_{\phi\phi}^g]^{-1}[k_{t\phi}^g]^T + [k_{t\psi}^g][k_{\psi\psi}^g]^{-1}[k_{t\psi}^g]^T \\ [K_2] &= [k_{tr}^g] + [k_{t\phi}^g][k_{\phi\phi}^g]^{-1}[k_{r\phi}^g]^T + [k_{t\psi}^g][k_{\psi\psi}^g]^{-1}[k_{r\psi}^g]^T \\ [K_3] &= [k_{rr}^g] + [k_{r\phi}^g][k_{\phi\phi}^g]^{-1}[k_{r\phi}^g]^T + [k_{r\psi}^g][k_{\psi\psi}^g]^{-1}[k_{r\psi}^g]^T \end{aligned} \tag{37}$$

The stability criterion is achieved based on neutral equilibrium method (Jadhav and Bajoria, 2013). According to this method, the corresponding load at which the structure attains equilibrium in both straight and the slightly bent configurations is defined as a critical load. The geometric matrix is represented by $\lambda[K_G]$, where λ is the scalar multiplier. The scalar multiplier is obtained such that the equilibrium is established for both the reference configuration $\{d_t\}$ and slightly deformed configuration $\{d_t\} + \{\delta d_t\}$(Jadhav and Bajoria, 2013)

$$([K] + \lambda[K_G])\{d_t\} = \{F_t\} \tag{38}$$

$$([K] + \lambda[K_G])(\{d_t\} + \{\delta d_t\}) = \{F_t\} \tag{39}$$

Subtracting equation (39) from equation (38) yields the eigenvalue problem

$$([K] + \lambda[K_G])\{\delta d_t\} = 0 \tag{40}$$

Here, the critical buckling load is the eigenvalue with the lowest magnitude, and the displacement vector $\{\delta d_t\}$ represents the corresponding buckled mode shape.

Table 1. Material properties of $BaTiO_3$ and $CoFe_2O_4$ (Moita et al., 2009).

Material	$C_{11} = C_{22}$ (10^9 N/m^2)	C_{12} (10^9 N/m^2)	$C_{13} = C_{23}$ (10^9 N/m^2)	C_{33} (10^9 N/m^2)	$C_{44} = C_{55}$ (10^9 N/m^2)	C_{66} (10^9 N/m^2)	ρ (kg/m^3)
$BaTiO_3$	166	77	78	162	43	44.5	5800
$CoFe_2O_4$	286	173	170.5	269.5	45.3	56.5	5800
$BaTiO_3$	$e_{31} = e_{32} = -4.4$ (C/m^2)	$e_{32} = 18.6$ (C/m^2)	$e_{24} = e_{15} = 11.6$ (C/m^2)	$\varepsilon_{11} = \varepsilon_{22} = 11.2$ (10^{-9} C/N m^2)	ε_{33} (10^{-9}C/N m^2) = 12.6	$\mu_{11} = \mu_{22} = 5$ (10^{-6} N s^2/C^2)	$\mu_{33} = 10$ (10^{-6} N s^2/C^2)
$CoFe_2O_4$	$q_{31} = q_{32}$ (N/A m) = 180.3	q_{33} (N/A m) = 699.7	$q_{24} = q_{15} = 550$ (N/A m)	$\varepsilon_{11} = \varepsilon_{22} = 0.08$ (10^{-9} C/N m^2)	$\varepsilon_{33} = 0.093$ (10^{-9} C/N m^2)	$\mu_{11} = \mu_{22} = -590$ (10^{-6} N s^2/C^2)	$\mu_{33} = 157$ (10^{-6}N s^2/C^2)

Results and discussion

Buckling analysis of layered SMEE plate is carried out to assess the nature of stability by forming an eigenvalue problem. Such eigenvalue problem yields eigenvalues, that is, critical buckling loads and their corresponding mode shapes in terms of eigenvectors. The multilayered SMEE plate involved in this study is made of piezoelectric ($BaTiO_3$) and magnetostrictive ($CoFe_2O_4$) material both being transversely isotropic. The material property of the SMEE composite is considered similar to Moita et al. (2009) as shown in Table 1. The non-dimensional critical buckling load for SMEE plate is given by $\lambda_{cr} = \lambda a^2/H^3 C_{11}$(where C_{11} corresponds to the largest elastic constant value of MEE material). The local skew coordinate of the SMEE plate is transformed to the global coordinate using a transformation matrix. Two types of stacking sequence are studied in this analysis. One being B/F/B, that is, the magnetostrictive layer is sandwiched between two piezoelectric layers, and the other sequence is F/B/F wherein the piezoelectric layer is sandwiched between two magnetostrictive layers. The stability characteristics of the SMEE plate are evaluated for different skew angles, aspect ratio, span-to-thickness ratio and boundary conditions. The effect of boundary conditions on the stability behaviour of the SMEE plate has been studied. The boundary conditions used in this analysis are CCCC (all sides clamped), CCCF (three clamped sides and one is free) and FCFC (two clamped and two free sides) and are given as follows

$$
\begin{aligned}
&\text{Clamped edge}\\
&\text{at } x = \tan\alpha, x = a + y\tan\alpha\\
&u_0^1 = v_0^1 = w_0^1 = \theta_x^1 = \theta_y^1 = \theta_z^1 = \phi^1 = \psi^1 = 0\\
&\text{at } y = 0, y = b\ \cos\ \alpha\\
&u_0 = v_0 = w_0 = \theta_x = \theta_y = \theta_z = \phi = \psi = 0\\
&\text{Free edge}\\
&\text{at } x = \tan\alpha, x = a + y\tan\alpha\\
&u_0^1 = v_0^1 = w_0^1 = \theta_x^1 = \theta_y^1 = \theta_z^1 = \phi^1 = \psi^1 \neq 0\\
&\text{at } y = 0, y = b\ \cos\ \alpha\\
&u_0 = v_0 = w_0 = \theta_x = \theta_y = \theta_z = \phi = \psi \neq 0\\
&\text{Simply} - \text{supportededge}\\
&\text{at } x = \tan\alpha, x = a + y\tan\alpha\\
&v_0^1 = w_0^1 = \theta_y^1 = \theta_z^1 = \phi^1 = \psi^1 = 0\\
&\text{at } y = 0, y = b\ \cos\ \alpha\\
&u_0 = w_0 = \theta_x = \theta_z = \phi = \psi = 0
\end{aligned}
\tag{41}
$$

Validation

To the best of authors' knowledge, research on buckling of layered SMEE plate is unavailable in the open literature. Hence, to validate the proposed FE formulation for solving a buckling problem, initially buckling analysis of

Table 2. Buckling load $\lambda_{cr} = \lambda a^2/H^3E_2$ for three-layered (0°/90°/0°) composite plate under in-plane load.

a/h ratio	Type of load	Non-dimensional critical buckling load				
		Reddy (2004)	This study			
			4 × 4	8 × 8	16 × 16	20 × 20
10	Uniaxial	15.2890	15.0319	14.8981	14.8694	14.8690
	Biaxial	7.6445	7.5159	7.4490	7.4347	7.4345
50	Uniaxial	22.9781	22.4591	22.1085	22.0464	22.0418
	Biaxial	11.4890	11.2295	11.0542	11.0232	11.0209
100	Uniaxial	23.3633	23.0521	22.9703	22.8492	22.8461
	Biaxial	11.6820	11.5260	11.4851	11.4246	11.4230

Table 3. Normalized natural frequencies $\bar{\omega} = \omega a\sqrt{\rho_{\max}/C_{\max}}/h$ of the BFB simply-supported plate with different *h/a* ratios.

h/a ratio	Approach	Non-dimensional natural frequency			
		1	2	3	4
10^{-1}	FSDT (Milazzo, 2016))	3.83	9.17	12.74	14.12
	ESL2 (Milazzo, 2016))	3.84	9.19	12.74	14.14
	ESL3 (Milazzo, 2016))	3.82	9.12	12.74	13.98
	ESL4 (Milazzo, 2016))	3.82	9.12	12.74	13.97
	LW1 (Milazzo, 2016))	3.90	9.30	12.74	14.26
	LW2 (Milazzo, 2016))	3.81	9.10	12.74	13.96
	LW3 (Milazzo, 2016))	3.81	9.11	12.74	13.96
	LW4 (Milazzo, 2016))	3.83	9.17	12.74	14.12
	This model	3.82	9.12	12.74	13.98
10^{-2}	FSDT (Milazzo, 2016))	3.95	9.89	15.82	19.93
	ESL2 (Milazzo, 2016))	3.96	9.91	15.86	19.97
	ESL3 (Milazzo, 2016))	3.96	9.91	15.85	19.97
	ESL4 (Milazzo, 2016))	3.96	9.91	15.85	19.96
	LW1 (Milazzo, 2016))	4.04	10.10	16.15	20.35
	LW2 (Milazzo, 2016))	3.95	9.89	15.82	19.92
	LW3 (Milazzo, 2016))	3.95	9.89	15.82	19.92
	LW4 (Milazzo, 2016))	3.95	9.89	15.82	19.92
	This model	3.95	9.84	15.79	19.87

FSDT: first-order shear deformation theory.

simply-supported multilayered laminate composite plate studied by Reddy (2004) has been considered. The necessary boundary condition is provided in equation (41). The material properties considered by Reddy (2004) are $E_1 = 25E_2, G_{12} = G_{13} = 0.5E_2, G_{23} = 0.2E_2$, $\vartheta_{12} = 0.25, k = 5/6$. In this regard, the coupled constitutive equations of the SMEE plate have been decoupled (by setting electric and magnetic effect to 0) and implemented for the analysis of laminated composite plate. Convergence studies were performed by considering different mesh sizes. For a mesh size of 20 × 20, the results obtained are well in agreement with the existing results (Reddy, 2004) as shown in Table 2. Hence, for all the subsequent analysis, a mesh size of 20 × 20 (400 elements) has been implemented. In addition, the effectiveness of this model in solving a multifield problem is assessed. In this regard, the free vibration behaviour of BFB MEE plate studied by Milazzo (2016) using refined kinematic models and Carrera unified formulation is considered for validation, and the corresponding results are presented in Table 3. The free vibration analysis presented in Table 3 is performed by considering the stiffness matrix and the mass matrix while the geometrical stiffness matrix is neglected. The results show a close agreement with each other. Furthermore, Table 4 depicts the stability behaviour of the simply-supported and clamped laminated skew composite plate (Chakrabarti and Sheikh, 2010; Hu and Tzeng, 2000) which is also studied to emphasize the correctness of the formulation for the study of skew plates. The material properties concerned with the skew composite plate are $E_1 = 128$ GPa, $E_2 = 11$ GPa, $G_{12} = G_{13} = 4.48$ GPa, $G_{23} = 1.53$ GPa, $\vartheta_{12} = 0.25$.

Effect of skew angle on buckling load

This section discusses the influence of skew angle (α) on the non-dimensional buckling load. The stability characteristics of the SMEE plate under different boundary conditions are investigated for skew angles

Table 4. Effect of skew angle on non-dimensional buckling load $\lambda_{cr} = \lambda a^2/H^3E_2$ for (90°/0°/0°/90°) cross-ply skew composite plate (a/b = 1; a/h = 100).

Skew angle (α)	Simply-supported			Clamped		
	Chakrabarti and Sheikh (2010)	Hu and Tzeng (2000)	This study (20 × 20)	Chakrabarti and Sheikh (2010)	Hu and Tzeng (2000)	This study (20 × 20)
0°	12.138	12.045	11.634	37.418	37.272	36.987
10°	13.020	13.000	12.635	38.798	38.180	37.613
20°	15.915	15.636	15.343	42.308	42.100	42.009
30°	21.605	21.500	20.669	49.274	49.000	48.894
40°	25.917	25.500	25.234	52.970	52.200	52.121

Table 5. Effect of skew angle on buckling load parameter $\lambda_{cr} = \lambda a^2/H^3C_{11}$ for B/F/B CCCC SMEE plate subjected to uniaxial compression (a/b = 1, a/h = 100).

Skew angle (α)	Buckling mode					
	1	2	3	4	5	6
0°	0.9399	3.0713	3.4003	5.4223	9.4127	10.1181
15°	1.0262	3.2248	3.7847	5.8462	10.1201	10.9020
30°	1.3436	3.9273	5.0607	7.4047	12.7022	13.7722
45°	2.1613	5.8867	8.2093	11.4246	19.3030	21.1458
60°	4.6567	12.0257	17.7547	23.7239	39.2709	43.5688

Table 6. Effect of skew angle on buckling load parameter $\lambda_{cr} = \lambda a^2/H^3C_{11}$ for B/F/B CCCF SMEE plate subjected to uniaxial compression (a/b = 1, a/h = 100).

Skew angle (α)	Buckling mode					
	1	2	3	4	5	6
0°	0.4289	1.8011	2.5949	3.8611	5.3537	7.1926
15°	0.4763	1.8980	2.8671	4.1142	5.8291	7.7097
30°	0.6517	2.2909	3.8311	5.0780	7.5396	9.6120
45°	1.1044	3.3787	6.2228	7.6547	11.8588	14.5250
60°	2.4842	6.7955	13.3330	15.7235	24.9038	29.5387

of 0°–60°. Table 5 presents the buckling load for CCCC SMEE plate with B/F/B stacking sequence subjected to uniaxial compression. It may be observed from Table 5 that the increase in skew angle effectively increases the buckling strength of the SMEE plate. The buckling modes witnessed a linear increase in buckling load with the increase in skew angle. Furthermore, Tables 6 and 7 display the effect of skew angle on buckling load for CCCF and FCFC SMEE plates, respectively. It may be observed from these tables (Tables 6 and 7) that the magnitude of buckling loads is reduced and it exhibits a similar trend as that of CCCC SMEE plate. In general, for all the considered boundary conditions, the buckling load increases with the increase in skew angle. However, the rate of increase in buckling load is observed to be higher for $\alpha = 45°$ and 60°. It may be due to the fact that stiffness of the SMEE plate increases at higher skew angles. The first three mode shapes corresponding to CCCC SMEE plate are presented in Figure 3 for $\alpha = 0°$, 30° and 60°. It may be noticed from Figure 3 that the formation of buckling mode (deformation) is shifting towards the corners of the SMEE plate with an increase in the skew angle.

Effect of uniaxial and biaxial compression

The effect of uniaxial and biaxial compression on the buckling behaviour of SMEE plate is concurrently investigated. Their influence on the stability characteristics is assessed on the basis of non-dimensional critical buckling load and with the corresponding modes. The SMEE plate having an aspect ratio of $a/b = 1$ and a span-to-thickness ratio of $a/h = 100$ with different boundary conditions is considered for the analysis. Table 8 presents a comparison between uniaxial and biaxial loading at a skew angle of $\alpha = 0°$, 30° and 45° in terms of non-dimensional critical buckling load. It can be observed from the results of Table 8 that the buckling loads get halved for the biaxial compression loading in comparison with the uniaxial loading case

Table 7. Effect of skew angle on buckling load parameter $\lambda_{cr} = \lambda a^2/H^3 C_{11}$ for B/F/B FCFC SMEE plate subjected to uniaxial compression (a/b = 1, a/h = 100).

Skew angle (α)	Buckling mode					
	1	2	3	4	5	6
0°	0.2519	0.8487	1.8595	2.7026	3.0422	3.7081
15°	0.2726	0.9002	2.0055	2.8625	3.3845	4.8989
30°	0.3767	1.1043	2.5460	3.4293	4.5842	6.4689
45°	0.6529	1.6538	3.9343	5.1042	7.4910	9.7709
60°	1.4970	3.3685	8.1144	10.4745	16.1308	19.8199

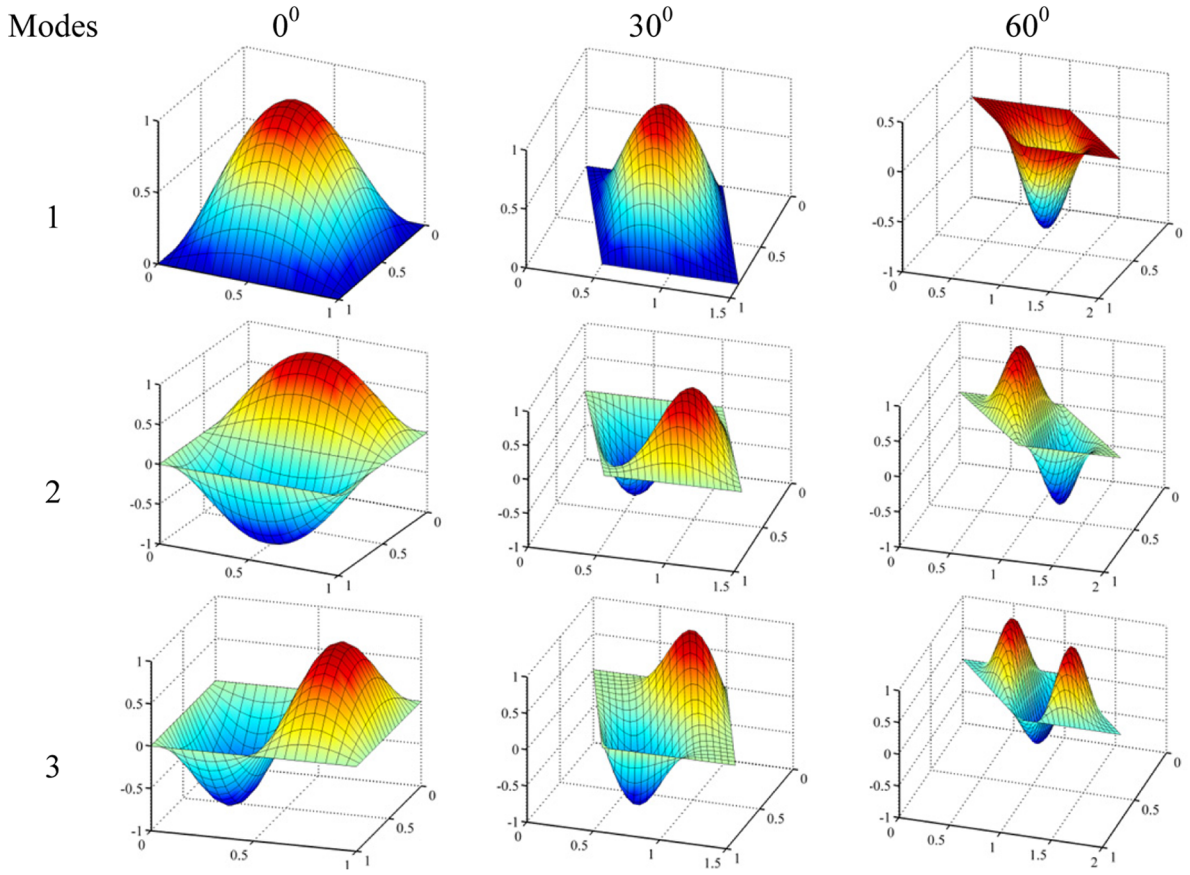

Figure 3. First three buckling modes at different skew angles for CCCC SMEE plate (a/b = 1, a/h = 100).

irrespective of skew angle and boundary conditions. This is due to the fact that the increase in the load decreases the buckling load of SMEE plate. The first three buckling modes are presented in Figure 4 for both the uniaxial and biaxial loading cases. The effect of uniaxial and biaxial loads on the mode shape of SMEE plate is significant and can be witnessed from the plate buckling direction in the figure.

Effect of material stacking sequence

The buckling behaviour of the SMEE plate is analysed for different stacking sequences of the SMEE plate. The two generally used stacking sequences (B/F/B and F/B/F) of the SMEE plate are considered for the analysis. Both the stacking sequences of SMEE plate are investigated under clamped–clamped boundary condition for α = 0°, 15°, 30° and 45° as shown in Figure 5. The SMEE plate having a/b = 1 and a/h = 100 is considered for the investigation. It may be observed from these plots that the SMEE plate with F/B/F stacking configuration yields higher critical buckling load than the B/F/B stacking configuration for all the skew angles of the SMEE plate. It may be due to the fact that the F/B/F configuration exhibits higher stiffness and hence larger buckling load. In addition, it may also be observed from Figure 5 that the non-

Table 8. Effect of uniaxial and biaxial compression on buckling load parameter $\lambda_{cr} = \lambda a^2/H^3C_{11}$ on B/F/B SMEE plate (a/b = 1, a/h = 100).

Boundary condition	Skew angle (α)	Buckling mode					
		1		2		3	
		Uniaxial	Biaxial	Uniaxial	Biaxial	Uniaxial	Biaxial
CCCC	0°	0.9399	0.4699	3.0713	1.5356	3.4000	1.7000
	30°	1.3436	0.6718	3.9273	1.9636	5.0600	2.5303
	45°	2.1613	1.0806	5.8867	2.9433	8.2093	4.1046
CCCF	0°	0.4289	0.2144	1.8011	1.5356	2.5949	1.7001
	30°	0.6517	0.3258	2.2909	1.1454	3.8311	1.1454
	45°	1.1044	0.5522	3.3787	1.6893	6.2228	3.1114
FCFC	0°	0.2519	0.1259	0.8487	0.4243	1.8595	0.9297
	30°	0.3767	0.1883	1.1043	0.5521	2.5460	1.2730
	45°	0.6529	0.3264	1.6538	0.8269	3.9343	1.9671

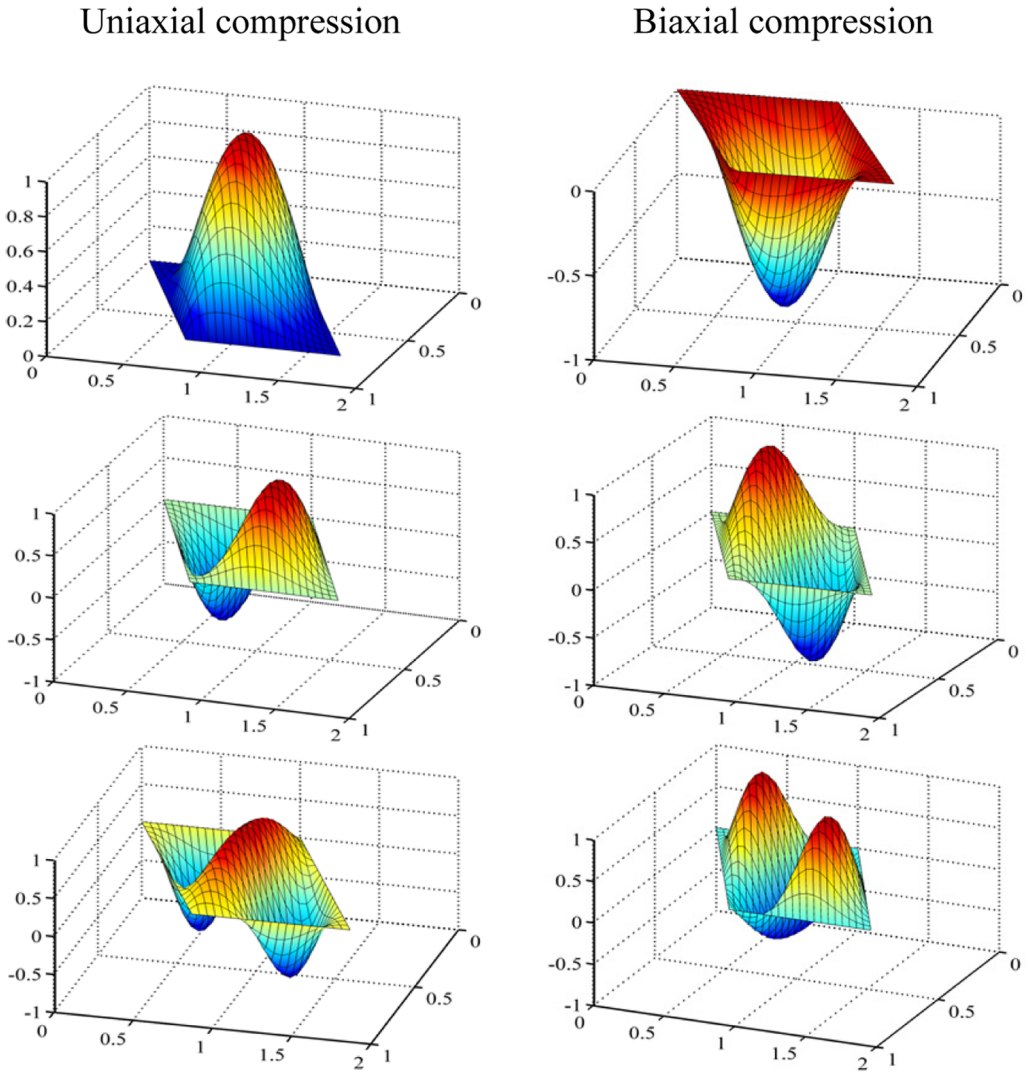

Figure 4. First three buckling modes for uniaxial and biaxial compression of CCCC SMEE plate (a/b = 1, a/h = 100, α = 45°).

dimensional buckling load for F/B/F plate was larger than B/F/B SMEE plate at α = 45° while for α = 0° the difference between two stacking sequences is minimum. Consequently, Figure 6 presents the comparison of first six buckling mode shapes for B/F/B and F/B/F stacking sequences. It can be seen that the

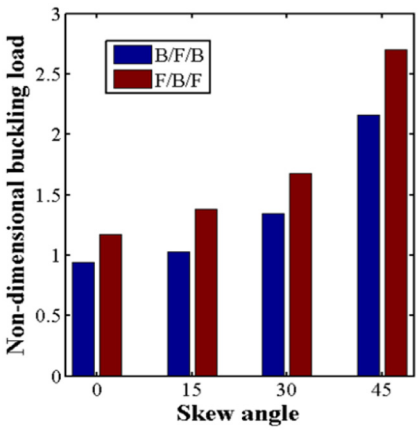

Figure 5. Non-dimensional buckling loads of CCCC SMEE plate subjected to uniaxial load for (a/b = 1, a/h = 100) BFB and FBF stacking.

increase in the stiffness of F/B/F plate influenced the mode shapes, and for higher buckling modes the effect is largely evident. The influence of material stacking sequence on the buckling mode shapes is presented in Figure 6. The higher buckling strength of FBF stacking over BFB SMEE plate can be witnessed from the mode shapes as higher buckling modes occur lately in case of SMEE plate with FBF stacking.

Effect of span-to-thickness ratio (a/h)

In this section, the effect of the span-to-thickness ratio (a/h) of the SMEE plate on the stability behaviour is investigated. Four different a/h ratios are studied, and their corresponding effect on the critical buckling load is analysed under uniaxial compression. Table 9 presents the critical buckling load for CCCC SMEE plate obtained for the span-to-thickness

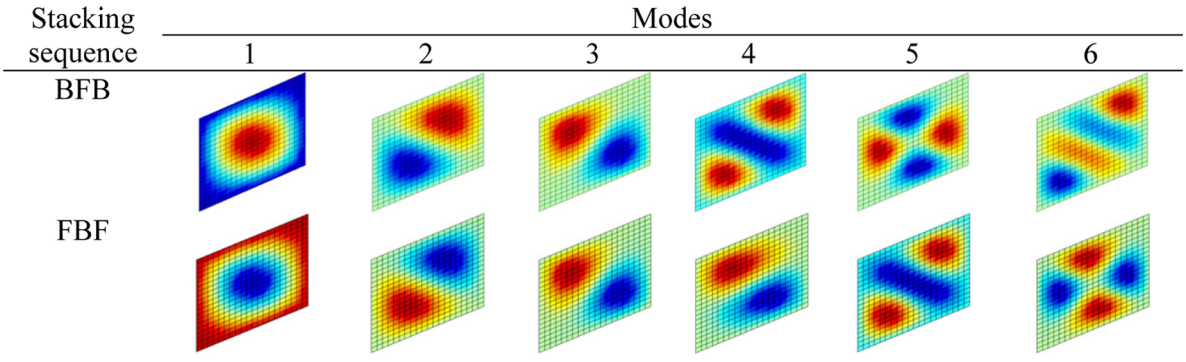

Figure 6. Influence of stacking sequence on buckling mode shapes of SMEE plate at α = 30° (a/b = 1, a/h = 100).

Table 9. Effect of thickness ratio on buckling load parameter $\lambda_{cr} = \lambda a^2/H^3 C_{11}$ of B/F/B CCCC SMEE plate (a/b = 1).

Skew angle (α)	a/h ratio	Buckling mode					
		1	2	3	4	5	6
0°	10	1.5726	4.4355	4.4520	7.3330	10.0748	11.2200
	20	1.3335	4.0207	4.1097	6.7823	9.8394	10.7785
	50	0.9368	3.0698	3.3987	5.4183	9.4011	10.0989
	100	0.9399	3.0713	3.4003	5.4223	9.4127	10.1181
15°	10	1.6767	4.4679	5.0402	7.7721	10.854	12.0721
	20	1.4268	4.0885	4.6403	7.2248	10.593	11.6063
	50	1.0262	3.2248	3.7847	5.8462	10.1204	10.9020
	100	1.0064	3.1599	3.7303	5.7352	10.0906	10.8688
30°	10	2.0624	5.1943	6.5973	9.3966	13.6671	15.2041
	20	1.7826	4.8095	6.1443	8.8586	13.3375	14.6686
	50	1.3436	3.9273	5.0607	7.4047	12.7022	13.7722
	100	1.3225	3.8632	4.9821	7.2729	12.6576	13.7227
45°	10	3.0660	7.3308	10.3528	13.6358	18.3952	20.7635
	20	2.7375	6.9491	9.80891	13.1198	20.3290	22.5895
	50	2.1613	5.8867	8.2093	11.4246	19.3030	21.1458
	100	2.1316	5.7957	8.0636	11.2150	19.2078	21.0333

Table 10. Effect of thickness ratio on buckling load parameter $\lambda_{cr} = \lambda a^2/H^3C_{11}$ of B/F/B CCCF SMEE plate (a/b = 1).

Skew angle (α)	a/h ratio	Buckling mode					
		1	2	3	4	5	6
0°	10	0.9435	2.5059	3.7801	5.4342	6.4487	9.3252
	20	0.7559	2.2533	3.4297	4.9257	6.0331	8.6186
	50	0.4213	1.7985	2.5832	3.8421	5.3298	7.1758
	100	0.4289	1.8011	2.5949	3.8611	5.3537	7.1926
15°	10	0.9962	2.6308	4.0610	5.6571	7.0538	9.8270
	20	0.8015	2.3661	3.7058	5.1548	6.5916	9.1304
	50	0.4763	1.8980	2.8671	4.1142	5.8291	7.7097
	100	0.4602	1.8722	2.8020	4.0350	5.7804	7.5970
30°	10	1.1940	3.0929	5.0926	6.6209	9.1180	11.7455
	20	0.9813	2.8012	4.7227	6.1130	8.5449	11.0674
	50	0.6517	2.2909	3.8311	5.0780	7.5396	9.6120
	100	0.6360	2.2626	3.7614	4.9979	7.4681	9.4843
45°	10	1.7182	4.3176	7.6965	9.3782	14.1269	15.0019
	20	1.4780	3.9999	7.3097	8.8526	13.4243	16.2599
	50	1.1044	3.3787	6.2228	7.6547	11.8588	14.5250
	100	1.0861	3.3399	6.1242	7.5444	11.7219	14.330

Table 11. Effect of thickness ratio on buckling load parameter $\lambda_{cr} = \lambda a^2/H^3C_{11}$ of B/F/B FCFC SMEE plate (a/b = 1)

Skew angle (α)	a/h ratio	Buckling mode					
		1	2	3	4	5	6
0°	10	0.7076	1.3169	2.7575	3.7778	3.9722	6.0262
	20	0.5405	1.1495	2.4184	3.4730	3.5930	5.2517
	50	0.2415	0.8231	1.8431	2.6986	3.0287	3.6974
	100	0.2519	0.8487	1.8595	2.7026	3.0422	3.7081
15°	10	0.7163	1.3779	2.9689	3.8842	4.3518	6.8440
	20	0.5474	1.2006	2.6245	3.5524	3.9876	6.1530
	50	0.2726	0.9002	2.0055	2.8625	3.3845	4.8989
	100	0.2590	0.8846	1.9618	2.8064	3.3496	4.7887
30°	10	0.8180	1.6077	3.5799	4.4185	5.7458	8.3122
	20	0.6399	1.4103	3.2170	4.0759	5.3160	7.6387
	50	0.3767	1.1043	2.5460	3.4293	4.5842	6.4689
	100	0.3644	1.0891	2.4999	3.3809	4.5341	6.3754
45°	10	1.1206	2.2101	5.0828	6.1620	9.1059	11.812
	20	0.9289	1.9906	4.6973	5.8240	8.5127	11.1107
	50	0.6529	1.6538	3.9343	5.1042	7.4910	9.7709
	100	0.6395	1.6361	3.8736	5.0454	7.4073	9.6400

ratios of a/h = 10, 20, 50 and 100 and a/b = 1. Furthermore, the analysis is extended to the CCCF and FCFC support conditions, and the corresponding results are tabulated in Tables 10 and 11, respectively. From the tabulated results in Tables 9 and 11, it may be observed that the critical buckling load increases for smaller thickness ratio, while with higher span-to-thickness ratio minimal influence is seen irrespective of the edge conditions and skew inclination of the SMEE plate.

Effect of aspect ratio (a/b)

The buckling behaviour of SMEE plate is studied for different aspect ratios. Figure 7(a) to (c) presents the non-dimensional critical buckling loads obtained for different aspect ratios at skew angles of 0°–60°. The results are obtained for a plate keeping thickness ratio of a/h = 100 and varying aspect ratio from 0.5 to 4 over an interval of 0.5. The decline in the buckling load is observed with the increase in aspect ratio as depicted in Figure 7(a). The decline in the buckling load is rapid for smaller aspect ratio, that is, $a/b < 2$, while for $a/b \geq 2$ a steady decline is observed. A similar trend is observed for the rest of the cases as shown in Figure 7(b) and (c). It is noteworthy to mention that for all the boundary conditions, the buckling load at $\alpha = 0°$ and $\alpha = 15°$ converged for $a/b \geq 1$, whereas in case of the FCFC boundary condition, the buckling load converged sharply for $a/b \geq 2.5$.

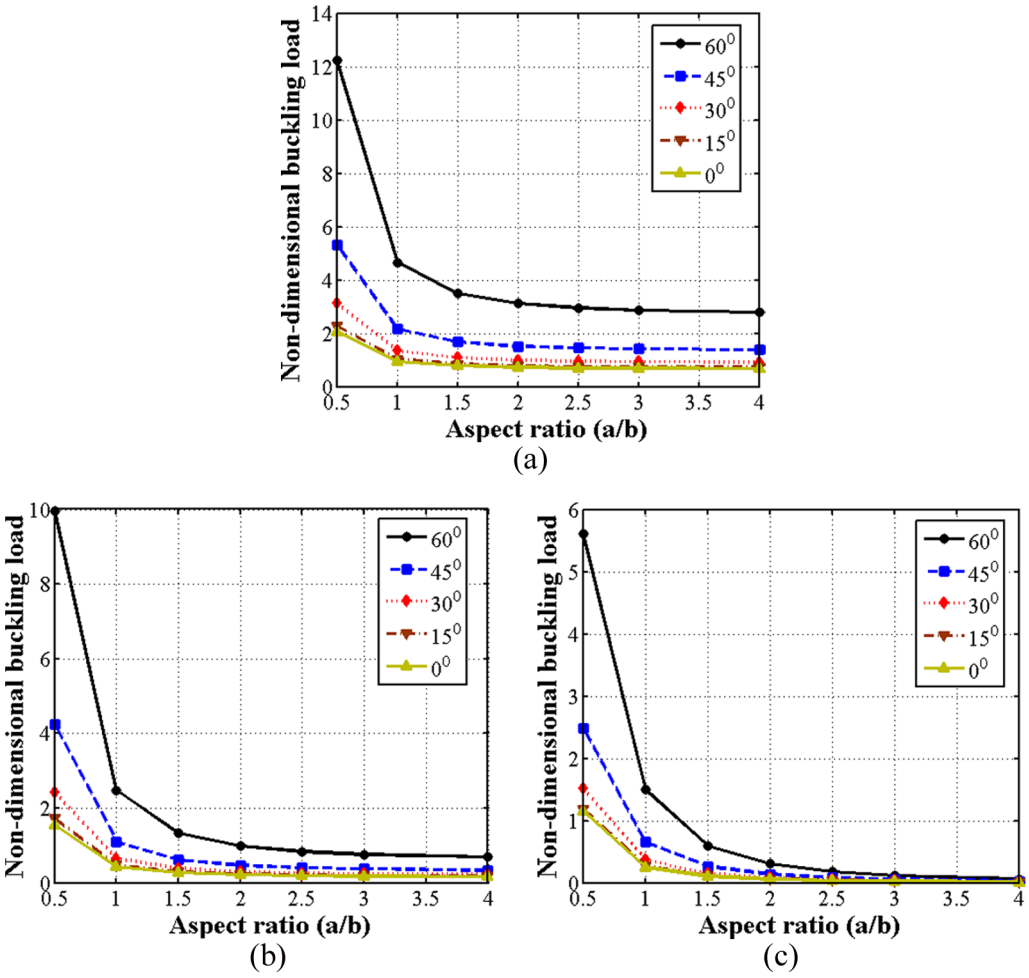

Figure 7. Effect of aspect ratio on buckling load parameter $\lambda_{cr} = \lambda a^2/H^3 C_{11}$ (a/h = 100): (a) CCCC, (b) CCCF and (c) FCFC.

Buckling behavioural study through mode shapes

The buckling behaviour of the SMEE plate influencing the buckling modes at various skew angles is demonstrated in Figure 8(a) to (d). In Figure 8, the effect of different boundary conditions on the non-dimensional buckling load for skew angles $\alpha = 0°$, 15°, 30° and 45° is considered while the plate dimensions are taken as $a/h = 100$ and $a/b = 1$. The effect of increase in skew angle affecting the buckling loads can be observed for all the three boundary conditions. However, the slope of CCCF plate is observed to be nearly constant for the first six modes at $\alpha = 0°$, 15° and 30°. Consequently, the effect of different boundary conditions on the respective mode shapes for $\alpha = 15°$ and 45° SMEE plate is demonstrated in Figure 9. In comparison with SMEE plate with $\alpha = 0°$, the introduction of skew angle caused the mode formation near to the plate corners for all three boundary conditions. It can also be observed from the figure that the number of half sine waves occurred is higher for $\alpha = 45°$ when compared with $\alpha = 15°$ for third to sixth modes. It can be stated observing from the figure that mode shapes are significantly influenced by skew angles introduced to SMEE plate. The increased influence on higher buckling mode shapes can be attributed to the increase in stiffness of SMEE plate. The increase in the stiffness of the SMEE plate at higher skew angles is due to the decrease in the plate area and a decrease in the perpendicular distance between the non-skew edges.

Conclusion

The buckling analysis of the layered SMEE plate is performed for the uniaxial and biaxial in-plane loadings. The skewness of the SMEE plate is achieved using a suitable transformation matrix. The displacement field corresponding to FSDT in conjunction with constitutive equations of MEE material is used to develop the FE model of the SMEE plate. The in-plane stress distribution within the SMEE plate existing due to the enacted force is considered to be equivalent to the applied in-plane compressive loads in the pre-buckling range. The corresponding stress distribution is used to derive the potential energy function. The important

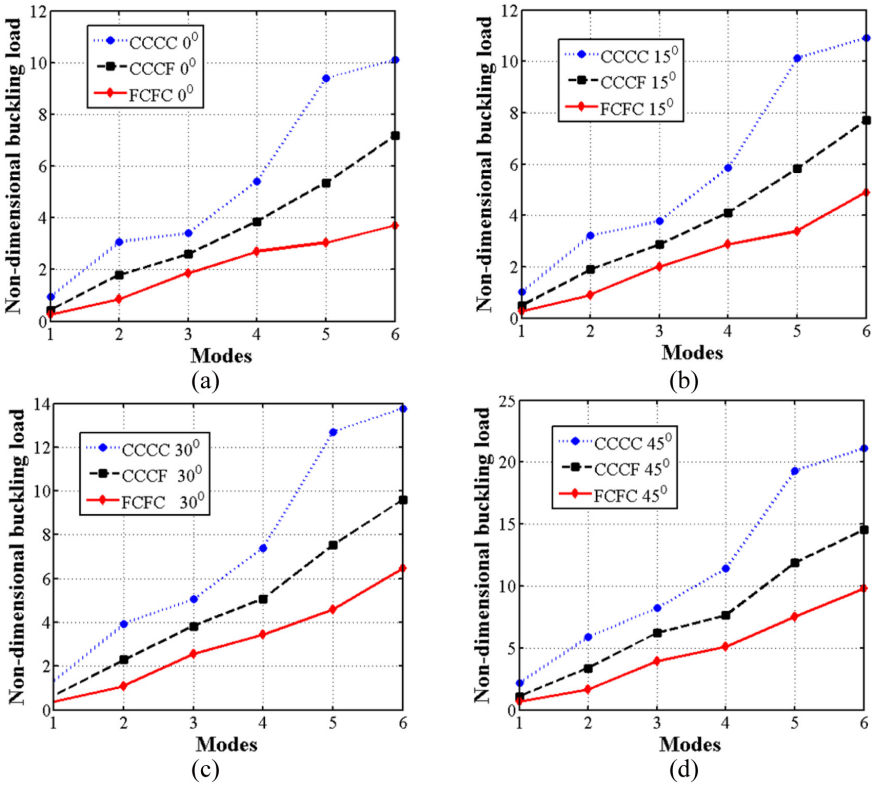

Figure 8. Effect of boundary condition on buckling load parameter $\lambda_{cr} = \lambda a^2/H^3 C_{11}$ (a/b = 1, a/h = 100): (a) α = 0°, (b) α = 15°, (c) α = 30° and (d) α = 45°.

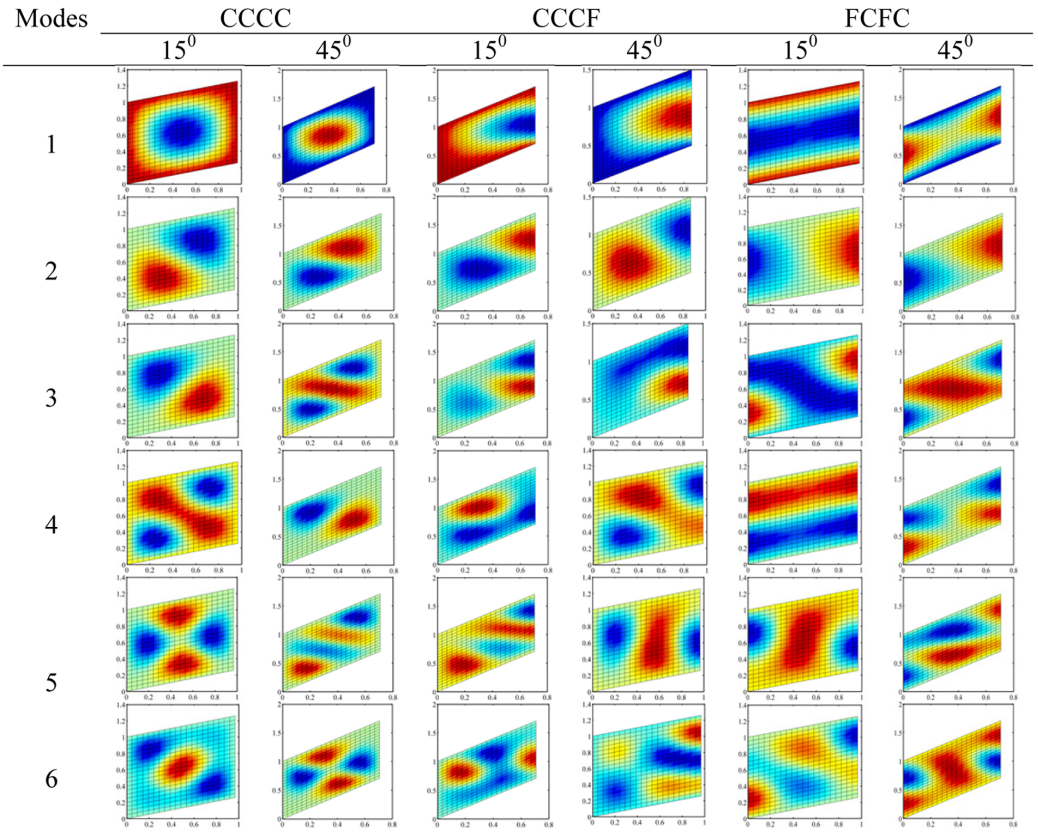

Figure 9. First six buckling modes of SMEE plate at skew angles α = 15° and α = 45°.

observations drawn from this analysis are the buckling strength increases with increase in the skew angle for all the boundary conditions. Furthermore, in case of biaxial loading, the buckling load is half of the uniaxial buckling load. The F/B/F stacking sequence of the SMEE plate displayed higher buckling strength over the B/F/B SMEE plate for all the skew angles. Higher span-to-thickness ratio has minimum influence on the buckling behaviour. In addition, the buckling load decreases with increase in aspect ratio of the SMEE plate irrespective of boundary conditions and skew angles. It is also observed that the influence of boundary condition is significant on the stability behaviour of the SMEE plate.

Declaration of conflicting interests

The author(s) declared no potential conflicts of interest with respect to the research, authorship and/or publication of this article.

Funding

The author(s) received no financial support for the research, authorship and/or publication of this article.

ORCID iD

Subhaschandra Kattimani https://orcid.org/0000-0002-2477-3783

References

Bhangale RK and Ganesan N (2005) Free vibration studies of simply supported non-homogeneous functionally graded magneto-electro-elastic finite cylindrical shells. *Journal of Sound and Vibration* 288: 412–422.

Boomgaard VJ and Born RA (1978) Sintered magnetoelectric composite material $BaTiO_3$-Ni (Co, Mn)Fe_2O_4. *Journal of Materials Science* 13(7): 1538–1548.

Buchanan GR (2004) Layered versus multiphase magneto-electro-elastic composites. *Composites B* 35(5): 413–420.

Carrera E, Brischetto S, Fagiano C, et al. (2009) Mixed multilayered plate elements for coupled magneto-electro-elastic analysis. *Multidiscipline Modeling in Materials and Structures* 5(3): 251–256.

Carrera E, Cinefra M and Li G (2018) Refined finite element solutions for anisotropic laminated plates. *Composite Structures* 183(1): 63–76.

Chakrabarti A and Sheikh AH (2010) Buckling of laminated composite plates by a new element based on higher order shear deformation theory. *Mechanics of Advanced Materials and Structures* 10(4): 303–317.

Chen JY, Heylige PR and Pan E (2014) Free vibration of three-dimensional multilayered magneto-electro-elastic plates under clamped/free boundary conditions. *Journal of Sound and Vibration* 333: 4017–4029.

Daripa R and Singha MK (2009) Influence of corner stresses on the stability characteristics of composite skew plates. *International Journal of Non-linear Mechanics* 44(2): 138–146.

Durvasula S (1971) Buckling of simply supported skew plates. *Journal of the Engineering Mechanics Division* 97(3): 967–979.

Ebrahimi F and Barati MR (2016a) Magnetic field effects on buckling behavior of smart size-dependent graded nanoscale beams. *European Physical Journal Plus* 131(7): 1–14.

Ebrahimi F and Barati MR (2016b) Magneto-electro-elastic buckling analysis of nonlocal curved nanobeams. *European Physical Journal Plus* 131(9): 346.

Ebrahimi F and Barati MR (2016c) Static stability analysis of smart magneto-electro-elastic heterogeneous nanoplates embedded in an elastic medium based on a four-variable refined plate theory. *Smart Materials and Structures* 25(10): 105014.

Ferreira AJM, Roque CMC, Neves AMA, et al. (2011) Buckling analysis of isotropic and laminated plates by radial basis functions according to a higher-order shear deformation theory. *Thin-Walled Structures* 49(7): 804–811.

Guan Q (2012) The free vibration of the magneto-electro-elastic materials laminated circular plate. *Advanced Materials Research* 374: 2193–2199.

Hu HT and Tzeng WL (2000) Buckling of skew laminate plates subjected to uniaxial inplane loads. *Thin-Walled Structures* 38: 53–77.

Jaberzadeh E and Azhari M (2014) Local buckling of moderately thick stepped skew viscoelastic composite plates using the element-free Galerkin method. *Acta Mechanica* 226(4): 1011–1025.

Jadhav P and Bajoria K (2013) Stability analysis of piezoelectric FGM plate subjected to electro-mechanical loading using finite element method. *International Journal of Applied Science and Engineering* 11(4): 375–391.

Jamalpoor A, Ahmadi-Savadkoohi A, Hossein M, et al. (2017) Free vibration and biaxial buckling analysis of double magneto-electro-elastic nanoplate-systems coupled by a visco-Pasternak medium via nonlocal elasticity theory. *European Journal of Mechanics* 63: 84–98.

Kattimani SC (2015) *Active control of geometrically nonlinear vibrations of magneto-electro-elastic plates and shells*. PhD Dissertation, IIT Kharagpur, Kharagpur, India.

Kattimani SC (2017) Geometrically nonlinear vibration analysis of multiferroic composite plates and shells. *Composite Structures* 163: 185–194.

Kattimani SC and Ray MC (2014a) Active control of large amplitude vibrations of smart magneto-electro-elastic doubly curved shells. *International Journal of Mechanics and Materials in Design* 10: 351–378.

Kattimani SC and Ray MC (2014b) Smart damping of geometrically nonlinear vibrations of magneto-electro-elastic plates. *Composite Structures* 114: 51–63.

Kattimani SC and Ray MC (2015) Control of geometrically nonlinear vibrations of functionally graded magneto-electro-elastic plates. *International Journal of Mechanical Sciences* 99: 154–167.

Kondaiah P, Shankar K and Ganesan N (2015) Pyroeffects on magneto-electro-elastic sensor bonded on mild steel cylindrical shell. *Smart Structures Systems* 16(3): 537–554.

Kondaiah P and Shankar K (2017) Pyroeffects on magneto-electro-elastic sensor patch subjected to thermal load. *Smart Structures and Systems* 19(3): 299–307.

Kumar R, Banerjee B and Ramachandra LS (2016) Nonlinear stability and dynamics of composite skew plates

under nonuniform loadings using differential quadrature method. *Mechanics Research 7Communication* 73: 76–90.

Kumaravel A, Ganesan N and Sethuraman R (2007) Buckling and vibration analysis of layered and multiphase magneto-electro-elastic beam under thermal environment. *Multidiscipline Modeling in Materials and Structures* 3(4): 461–476.

Kumaravel A, Ganesan N and Sethuraman R (2010) Buckling and vibration analysis of layered and multiphase magneto-electro-elastic cylinders subjected to uniform thermal loading. *Multidiscipline Modeling in Materials and Structures* 6(4): 475–492.

Lage RG, Soares CMM, Soares CAM, et al. (2004) Layerwise partial mixed finite element analysis of magneto-electro-elastic plates. *Computers and Structures* 82: 1293–1301.

Li YS (2014) Buckling analysis of magnetoelectroelastic plate resting on Pasternak elastic foundation. *Mechanics Research Communication* 56: 104–114.

Li YS, Ma P and Wang W (2016) Bending, buckling, and free vibration of magnetoelectroelastic nanobeam based on nonlocal theory. *Journal of Intelligent Material Systems and Structures* 27(9): 1139–1149.

Liu J, Zhang P, Lin G, et al. (2016) Solutions for the magneto-electro-elastic plate using the scaled boundary finite element method. *Engineering Analysis with Boundary Elements* 68: 103–114.

Milazzo A (2014a) Large deflection of magneto-electro-elastic laminated plates. *Applied Mathematical Modelling* 38(5): 1737–1752.

Milazzo A (2014b) Refined equivalent single layer formulations and finite elements for smart laminates free vibrations. *Composites B* 61: 238–253.

Milazzo A (2016) Unified formulation for a family of advanced finite elements for smart multilayered plates. *Mechanics of Advanced Materials and Structures* 23(9): 971–980.

Mizusawa T, Kajita T and Naruoka M (1998) Buckling of skew plate structures using B-spline functions. *International Journal for Numerical Methods in Engineering* 15(1): 87–96.

Moita JMS, Soares CMM and Soares CAM (2009) Analyses of magneto-electro-elastic plates using a higher order finite element model. *Composite Structures* 91: 421–426.

Ottavio MD and Carrera E (2010) Variable-kinematics approach for linearized buckling analysis of laminated plates and shells. *AIAA J* 48: 1987–1996.

Pan E (2001) Exact solution for simply supported and multilayered magneto-electro-elastic plates. *Journal of Applied Mechanics* 68: 608–618.

Pan E and Han F (2005) Exact solutions for functionally graded and layered magneto-electro-elastic plates. *International Journal of Engineering Science* 43: 321–339.

Pan E and Heyliger PR (2002) Free vibration of simply supported and multilayered magnetoelectro-elastic plates. *Journal of Sound and Vibration* 252(3): 429–442.

Pan E and Heyliger PR (2003) Exact solutions for magneto-electro-elastic laminates in cylindrical bending. *International Journal of Solids and Structures* 40(24): 6859–6876.

Ramirez F, Heyliger PR and Pan E (2006) Free vibration response of two-dimensional magneto-electro-elastic plates. *Journal of Sound and Vibration* 292: 626–644.

Reddy JN (2004) *Mechanics of Laminated Composite Plates and Shells: Theory and Analysis*. Boca Raton, FL: CRC Press.

Upadhyay AK and Shukla KK (2013) Post-buckling behaviour of composite and sandwich skew plates. *International Journal of Nonlinear Mechanics* 55: 120–127.

Upadhyay AK and Shukla KK (2014) Post-buckling analysis of skew plates subjected to combined in-plane loadings. *Acta Mechanica* 225(10): 2959–2968.

Van Suchtelen J (1972) Product properties: a new application of composite materials. *Philips Research Report* 27: 28.

Vinyas M and Kattimani SC (2017a) A finite element based assessment of static behavior of multiphase magneto-electro-elastic beams under different thermal loading. *Structural Engineering Mechanics* 62(5): 519–535.

Vinyas M and Kattimani SC (2017b) Static analysis of stepped functionally graded magneto-electro-elastic plates in thermal environment: a finite element study. *Composite Structures* 178: 63–86.

Vinyas M and Kattimani SC (2017c) Static studies of stepped functionally graded magneto-electro-elastic beam subjected to different thermal loads. *Composite Structures* 163: 216–237.

Wang CM, Liew KM and Alwis WAM (1992) Buckling of skew plates and corner condition for simply supported edges. *Journal of Engineering Mechanics* 118(4): 651–662.

Wang J, Chen L and Fang S (2003) State vector approach to analysis of multilayered magneto-electro-elastic plates. *International Journal of Solids and Structures* 40: 1669–1680.

Wang S (1997) Buckling analysis of skew fibre-reinforced composite laminates based on first-order shear deformation plate theory. *Composite Structures* 37(1): 5–19.

Xu XJ, Deng ZC, Zhang K, et al. (2016) Surface effects on the bending, buckling and free vibration analysis of magneto-electro-elastic beams. *Acta Mechanica* 227(6): 1557–1573.